Accurate Time-Domain Simulation of Nonlinear Inductors Including Hysteresis and Eddy-Current Effects

Lucian MANDACHE, Dumitru TOPAN, Ioana Gabriela SIRBU

***Abstract*—This paper proposes an accurate time-domain model of nonlinear inductor with hysteresis and eddy-current losses. The diagram model is based on analog lumped equivalent circuits and the implementation procedure uses the principle of modularity. The complete model is conceived as a SPICE subcircuit which includes the coil leakage inductance, the winding resistance, the eddy-current effect and the ferromagnetic hysteresis based on the Jiles - Atherton model. Normal operation modes, as well as critical transients and faulty situations can be simulated as fully as possible using the presented model.**

***Index Terms*—Time-domain simulation, ferromagnetic hysteresis, eddy-current, nonlinear magnetics**

I. Introduction

THE ferromagnetic cores are basic constructive elements of transformers and inductors for wide application area, ranging from analog and digital microelectronics toward power converters and power systems. It is known that the rigorous study and design optimization of such electromagnetic devices is difficult because of nonlinearity, electromagnetic inertial behavior and other related phenomena, as saturation, anisotropy, magnetic hysteresis and induced eddy currents.

The optimal design of devices requires the consideration of the whole electromagnetic system, including the power supply and the load, in rated operation mode as well as in malfunction modes. This is possible by means of a computer aided design, based on an adequate modeling and simulation using software tools capable to provide the analysis of the entire equipment with adequate accuracy. Even though co-simulation solutions involving a FEM-based simulator, for the electromagnetic and thermal analysis, and a time-domain circuit simulator could offer the most accurate results [1,2], they are obviously the most expensive ones regarding hardware and software requirements, computation effort and simulation time and last but not least the high level qualification of the design engineer.

In this context, in order to achieve reasonable design costs with reasonable accurate results, the paper proposes an accurate time-domain model of nonlinear inductors. It can be supplied by harmonic or distorted voltages.

The procedure uses the concept of modeling the whole electromagnetic system through equivalent diagrams with lumped circuits, so that only one simulation software is necessary. The FEM-based analysis is therefore avoided. The modeling solution is SPICE-compatible, so that the mathematical model is reduced to a nonlinear differential-algebraic equation system. This modeling and simulation principle has been promoted previously by some authors [3-8].

We paid special attention to conceive the modeling and simulation method so that it would become a really useful tool for researchers and designers. In principle, almost any circuit simulator can be used as software environment.

The modeling procedure follows the specific phenomena related to the wired ferromagnetic pieces, explained by the Maxwell's equations.

The ferromagnetic piece model combines the nonlinearity with saturation, magnetic hysteresis and induced eddy-current.

The modeling procedure has a wide range of generality, being suitable to be extended to transformers, linear actuators and rotating motors.

II. Modeling of Eddy-Current Losses

A coil with ferromagnetic core including an airgap, whose winding has N turns, the electric resistance R and the leakage inductance L_w, admits the equivalent diagram shown in fig. 1, where $\varphi(t)$ is the main fascicular magnetic flux and $i_L(t)$ is the current required from the independent voltage source $u_s(t)$.

The circuit equation is

$$Ri_L + L_w \frac{\mathrm{d}i_L}{\mathrm{d}t} + N\frac{\mathrm{d}\varphi}{\mathrm{d}t} = u_s, \qquad (1)$$

which suggests that a linear inductor of resistance R and inductance L_w is connected in series with a nonlinear inductor, whose ferromagnetic core involves nonlinear hysteresis and eddy-current losses.

Manuscript received March 23, 2011.
This work was supported by The Romanian Ministry of Education, Research, Youth and Sport - CNCS - UEFISCDI, project number 678/2009 PNII - IDEI code 539/2008.

Lucian Mandache is with the University of Craiova, Faculty of Electrical Engineering, Decebal Blv. 107, Craiova 200440, Romania (e-mail: lmandache@elth.ucv.ro).
Dumitru Topan is with the University of Craiova, Faculty of Electrical Engineering, Decebal Blv. 107, Craiova 200440, Romania (e-mail: dtopan@central.ucv.ro).
Ioana Gabriela Sirbu is with the University of Craiova, Faculty of Electrical Engineering, Decebal Blv. 107, Craiova 200440, Romania (e-mail: osirbu@elth.ucv.ro).

ISBN: 978-988-19251-4-5
ISSN: 2078-0958 (Print); ISSN: 2078-0966 (Online)

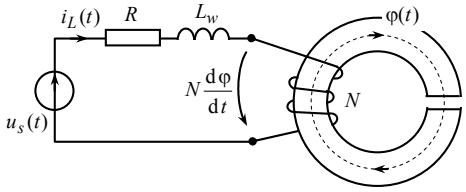

Fig. 1. Nonlinear inductor.

Assuming a uniform distribution of the magnetic field within the cross section of area A, the core flux is $\varphi(t) = B(t)A$, where $B(t)$ is the flux density. If the reactance of eddy-current path is neglected, its contribution on the magnetization of the inductor core is equivalent with a current

$$i_e(t) = K\frac{d\varphi}{dt}, \tag{2}$$

where $K > 0$ is a constant factor directly proportional to the mean length l of the core and inversely proportional to the core material resistivity ρ [8,9].

For any shape of the core cross section, the total eddy-current and its instantaneous power loss are obtained

$$i_e(t) = K_1\frac{l}{\rho}\cdot\frac{dB}{dt}, \tag{3}$$

$$p_e(t) = K_2\frac{l}{\rho}\cdot\left(\frac{dB}{dt}\right)^2 = K_2\frac{l}{\rho A^2}\cdot\left(\frac{d\varphi}{dt}\right)^2, \tag{4}$$

where K_1 and K_2 are constant factors depending on the core geometry, theirs corresponding formulae being established [8,9] for any shape of the core cross section, as well as for certain particularly cases (cylinder, silicon steel sheet, layered steel sheets).

The equivalent resistance defined as

$$R_e = \frac{p_e}{i_e^2} \tag{5}$$

is associated to the current i_e and to the losses p_e. It results

$$R_e = \frac{K_2}{K_1^2}\cdot\frac{\rho}{l}, \tag{6}$$

and the instantaneous eddy-current losses can be computed as the electromagnetic power required by this resistance:

$$p_e(t) = R_e i_e^2(t) = u_e(t)\cdot i_e(t), \tag{4'}$$

where the corresponding voltage drop appears.

The resistivity ρ of the core is specified by the manufacturer or can be computed using other technical data provided by the manufacturer: specific power losses p_0 [W/kg] corresponding to a sinusoidal working regime in the linear zone of the magnetization characteristic, for a reference frequency f_0 and a peak value of flux density B_0, as well as the mass density of the ferromagnetic material γ [8,9].

The modeling diagram of eddy-current losses, built according to the equations (2) and (5), is shown in fig. 2, where the control conductance of the controlling source is numerically equal to the constant factor K and computed for each particular case; we already treated certain cases of interest in engineering practice [8,9]. The diagram of figure 2 will be enclosed in the whole model of the nonlinear coil.

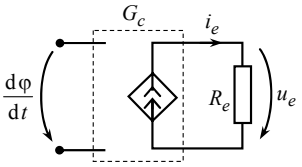

Fig. 2. Modeling diagram of eddy-current losses.

III. Modeling the Hysteresis and its Power Loss

The law of relationship between the flux density $\boldsymbol{B}$, magnetic field strength $\boldsymbol{H}$ and magnetization $\boldsymbol{M}$, valid in any point of the magnetic core, $\boldsymbol{B} = \mu_0(\boldsymbol{H} + \boldsymbol{M})$, leads to the expression of the magnetic flux in terms of local quantities:

$$\varphi = \mu_0 A(H + M), \tag{7}$$

where μ_0 is the permeability of free space. Due to the magnetic hysteresis, the magnetization is not entirely reversible, but it involves an irreversible component, too [10,11]. The irreversible component was exemplarily described by the Jiles-Atherton model of hysteresis, from where the total magnetic susceptibility has been derived:

$$\frac{dM}{dH} = \frac{M_{an} - M}{k\delta - \frac{\alpha}{1-c}\cdot(M_{an} - M)} + c\frac{dM_{an}}{dH}. \tag{8}$$

The expression (8) contains the anhysteretic component M_{an} of the magnetization corresponding to the initial magnetization curve of the ferromagnetic material, the anhysteretic susceptibility dM_{an}/dH and the coefficients α, c, k defining the shape of the hysteresis cycle and assessed starting from the physical characteristics of the material [10]. The coefficient δ is the sign factor designating the sense of variation of the excitation magnetizing force with respect to time [10].

The anhysteretic magnetization characteristic is obtained as lookup table starting from the manufacturer specifications. For simulation purposes, it would be more advantageous to use an analytical approximation in order to avoid possible discontinuities of the anhysteretic susceptibility. The most preferred analytical approximation is based on the modified Langevin function [5,10]:

$$M_{an} = \begin{cases} M_{sat}\left(\coth\frac{H_{ef}}{a} - \frac{a}{H_e}\right); \text{ if } H_{ef} \neq 0 \\ M_{sat}\cdot\frac{H_{ef}}{3a}; \text{ if } H_{ef} \to 0 \end{cases} \tag{9}$$

where the dependence is expressed in terms of the effective magnetizing strength $H_{ef} = H + \alpha M$. The shape

ISBN: 978-988-19251-4-5
ISSN: 2078-0958 (Print); ISSN: 2078-0966 (Online)

factor a depends on the peak magnetic permeability and the saturation magnetization M_{sat} depends on the saturation flux density, both parameters being extracted from the material datasheet. This analytical approximation allows expressing the anhysteretic susceptibility required by (8):

$$\frac{\mathrm{d}M_{an}}{\mathrm{d}H}=\begin{cases} M_{sat}\cdot\left(-\dfrac{1}{a\cdot\sinh^2\dfrac{H_{ef}}{a}}+\dfrac{a}{H_{ef}^2}\right);\ \text{if } H_{ef}\neq 0 \\ M_{sat}\cdot\dfrac{1}{3a};\ \text{if } H_{ef}\to 0 \end{cases} \tag{10}$$

In order to include the hysteresis model in a time-domain simulation program like SPICE, the solution of the differential equation (8) can be obtained only if the time is the independent variable. Therefore, since M and H are time-dependent, the expression below is obvious:

$$\frac{\mathrm{d}M(H(t))}{\mathrm{d}t}=\frac{\mathrm{d}M}{\mathrm{d}H}\cdot\frac{\mathrm{d}H}{\mathrm{d}t}. \tag{11}$$

By replacing (8) in (11), a more useful expression of the hysteresis model is obtained:

$$\frac{\mathrm{d}M}{\mathrm{d}t}=\left[\frac{M_{an}-M}{k\delta-\dfrac{\alpha}{1-c}\cdot(M_{an}-M)}+c\frac{\mathrm{d}M_{an}}{\mathrm{d}H}\right]\cdot\frac{\mathrm{d}H}{\mathrm{d}t}. \tag{12}$$

For any time-dependent function $H(t)$, the magnetization $M(t)$ is obtained by integrating (12) and the flux density $B(t)$ is simply computed with (7). If a periodic operation mode is assumed, with the fundamental frequency f and period $T=1/f$, the volume density of hysteresis loss energy that depends on the area bounded by one cycle of hysteresis $B(H)$ can be calculated as

$$w_H=\int\limits_{\substack{One\\cycle}}H\cdot\mathrm{d}B=\int\limits_0^{1/f}H\frac{\mathrm{d}B}{\mathrm{d}t}\cdot\mathrm{d}t\quad\left[\frac{\mathrm{J}}{\mathrm{m}^3}\right], \tag{13}$$

the corresponding power loss for the whole ferromagnetic piece of volume V_{Fe} being:

$$P_H=\frac{V_{Fe}}{T}\cdot\int\limits_{\left(\substack{One\\cycle}\right)}H\cdot\mathrm{d}B\quad[\mathrm{W}]. \tag{14}$$

Since the time-dependent quantities are already available, the more useful expression is obtained:

$$P_H=\frac{V_{Fe}}{T}\cdot\int_0^T H\frac{\mathrm{d}B}{\mathrm{d}t}\cdot\mathrm{d}t\quad[\mathrm{W}], \tag{15}$$

For constant cross-section along the ferromagnetic piece, so that $V_{Fe}=l\cdot A$, with the previous assumption on the uniform distribution of the magnetic field within the cross section, the expression (15) becomes:

$$P_H=f\cdot\int_0^T(Hl)\cdot\frac{\mathrm{d}\varphi}{\mathrm{d}t}\cdot\mathrm{d}t=f\cdot\int_0^T p_H(t)\cdot\mathrm{d}t, \tag{16}$$

where the instantaneous hysteresis power loss $p_H(t)$ was emphasized. It is extremely useful to assess hysteresis losses for any operation modes, including those that involve biases with a DC or low-frequency premagnetization and minor magnetization loops.

IV. Whole Model of the Nonlinear Inductor

The Ampere's law written for the nonlinear inductor of fig. 1, gives

$$Hl+H_a l_a=Ni_L-i_e, \tag{17}$$

where the subscript a denotes the quantities corresponding to the airgap. If the magnetic voltage drop on the airgap is expressed in terms of the flux and magnetic reluctance R_{ma}:

$$H_a l_a=\frac{B}{\mu_0}\cdot l_a=BA\cdot\frac{l_a}{\mu_0 A}=\varphi R_{ma}, \tag{18}$$

the expression (17) becomes:

$$Hl+\varphi R_{ma}=Ni_L-K\frac{\mathrm{d}\varphi}{\mathrm{d}t}, \tag{19}$$

where the equivalent eddy-current has been replaced according to (2). The equation (19) explains the modeling of the magnetic circuit using an equivalent analog circuit, as in fig. 3, where the magnetomotive forces are modeled through controlled voltage sources. The magnetic reluctance of the airgap is modeled through a linear electric resistance, while the ferromagnetic piece described by the equation of hysteresis (12) needs a separate model. Since the equations (1) and (19) are linked through common variables, the model diagram of the magnetic circuit is presented in conjunction to the model of the winding described by (1).

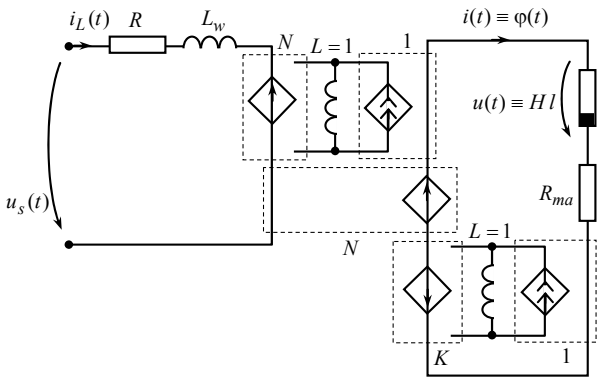

Fig. 3. Modeling diagram of electric circuit and magnetic circuit of the nonlinear inductor.

The time derivatives of the magnetic flux were obtained as voltages across unity-inductance inductors flowed by currents numerically equal to the flux.

The proposed model of the ferromagnetic piece with hysteresis is shown in fig. 4. Envisaging a SPICE implementation, and to reduce the circuit complexity,

ISBN: 978-988-19251-4-5
ISSN: 2078-0958 (Print); ISSN: 2078-0966 (Online)

nonlinear dependent sources were preferred [13]. By means of dependent sources, the equations (7), (9), (10) and (12) were modeled. Only the most important dependent sources are shown in fig. 4, where the corresponding equations are written in parentheses nearby each source. The quantities of interest are currents or voltages and they are used as controlling quantities for the nonlinear dependent sources. The unity-capacitance capacitor plays the role of integrator for its current numerically equal to $\mathrm{d}M/\mathrm{d}t$, in order to obtain the voltage numerically equal to the magnetization. One linear dependent source was used too and an inductor to obtain the time derivative of H.

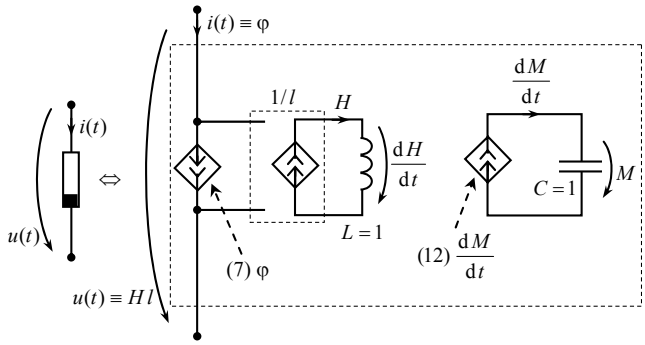

Fig. 4. Modeling diagram of the ferromagnetic piece with hysteresis.

In order to compute the instantaneous and mean power losses (both eddy-current and hysteresis), an additional diagram must be attached to the models of fig. 3 and 4. It is conceived as in fig. 5, where two nonlinear dependent current sources were used to give the instantaneous losses according to equations (4') and (16). The controlling quantities ($\mathrm{d}\varphi/\mathrm{d}t$ and Hl) are taken from the model diagram of fig. 3. Since the instantaneous power losses are obtained in any moment of the analysis time, the mean power losses are computed by integrating them along the analysis time. Such a procedure is more general than the integration within a time period expressed by (16). This is performed through linear capacitors with the capacitance numerically equal to the analysis time (noted T_a on the diagram).

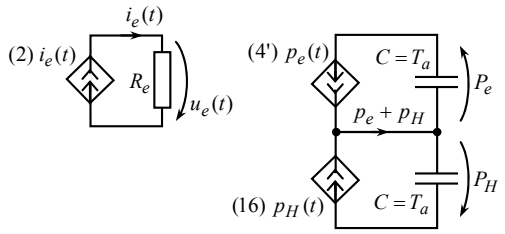

Fig. 5. Modeling diagram of the iron losses computation.

The copper instantaneous $p_J(t)$ and mean P_J losses in the winding resistance R are treated in similar manner. For the design optimization all categories of losses must be carefully assessed. The whole power loss P including copper and iron losses can be simply computed as:

$$P = f\int_0^T p(t)\cdot \mathrm{d}t = f\int_0^T u_s(t) i_L(t)\cdot \mathrm{d}t \qquad (20)$$

or rather

$$P = \frac{1}{T_a}\int_0^{T_a} p(t)\cdot \mathrm{d}t \ . \qquad (20')$$

V. Model Implementation and Example

The nonlinear inductor model developed above was implemented as a unique subcircuit in SPICE [13]. It integrates all three model diagrams shown in fig. 3, 4 and 5. Only the pair of inductor terminals remains accessible. Some quantities are extracted outside the subcircuit for postprocessing or saving in the output file (as the fascicular flux and the losses). The subcircuit parameters are all the constructive and material characteristics, including the constant factors used by the hysteresis model.

The inductor chosen as example has a E+I type core of layered silicon steel sheets with a carefully chosen airgap, conceived for an inductance of 1H at 0.3A and 50Hz. It has been directly connected to a sinusoidal voltage source. In the simulation SPICE diagram are included the elements of the network impedance (fig. 6).

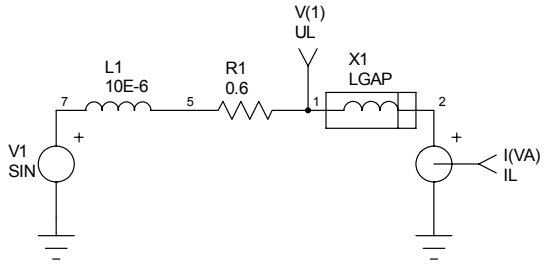

Fig. 6. SPICE simulation diagram.

Any working condition can be simulated, and any quantity can be computed and postprocessed. Our study is focused mainly on the management of the nonlinearity, magnetic hysteresis and eddy-current induced in the iron core, as well as on the assessment of iron losses. Some results are presented below. In the figure 7, the inductor current (curve 1) is shown together with the voltage (curve 2) at 50Hz; the distorted shape of the current denotes that the saturation level has been reached.

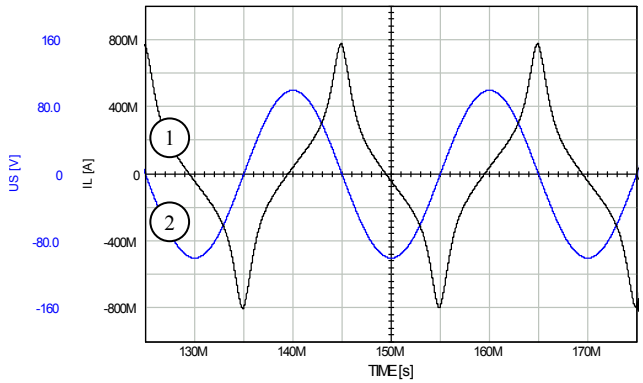

Fig. 7. Inductor current (1) and voltage (2).

ISBN: 978-988-19251-4-5
ISSN: 2078-0958 (Print); ISSN: 2078-0966 (Online)

The figure 8 shows the magnetization characteristic obtained for a damped voltage of the power source at 50Hz. The curve 1 emphasizes the effect of the magnetic hysteresis only (with ignoring the eddy-current), while the curve 2 includes the effect of eddy-current.

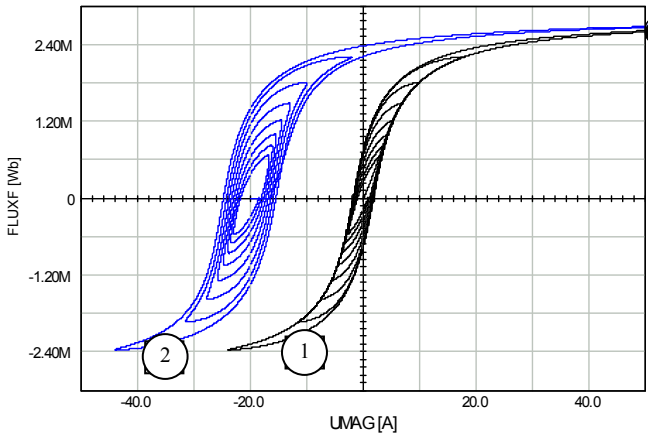

Fig. 8. Magnetization cycle of the iron core for damped supplying voltage: with hysteresis (1); with hysteresis and eddy-current (2).

In the figure 9 the effect of the airgap is shown if the inductor is supplied with a sinusoidal source of 50Hz.

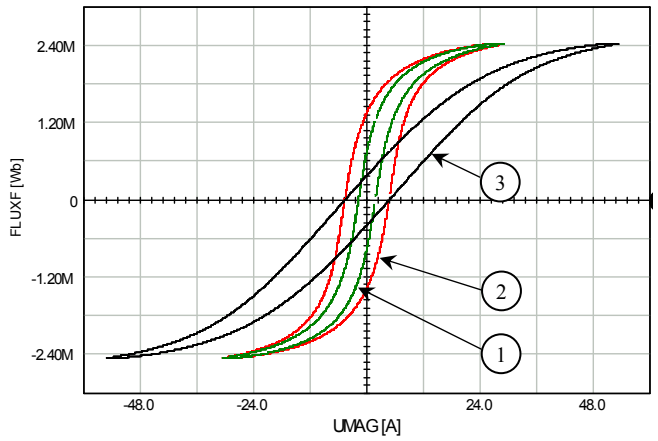

Fig. 9. Magnetization cycles: for the iron core with hysteresis (1); for the iron core with hysteresis and eddy-current (2); for the whole magnetic circuit, including the airgap (3).

The figure 10 shows the instantaneous power losses (iron and copper) at 50Hz.

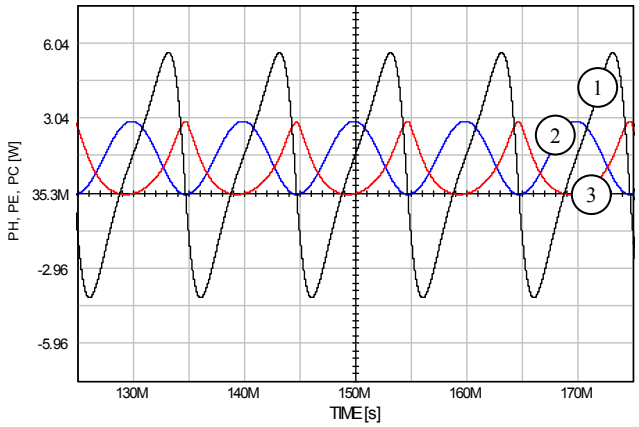

Fig. 10. Instantaneous power losses of the inductor at 50Hz: hysteresis loss (1); eddy-current loss (2); copper loss (3).

The figure 11 shows the influence of the frequency on the magnetization cycles including eddy-current. The corresponding mean values of the iron losses are given in the table 1. The peak value of the flux density was maintained at 1.52T for each operation frequency by adapting the amplitude of the supplying voltage so that the ratio V/f remains constant.

TABLE I. Mean values of the iron losses at certain frequencies.

f [Hz]	50	100	200	500	1000
P_H [W]	0.899	1.8	3.6	9.0	18.0
P_e [W]	1.495	5.98	23.94	149.6	598.2

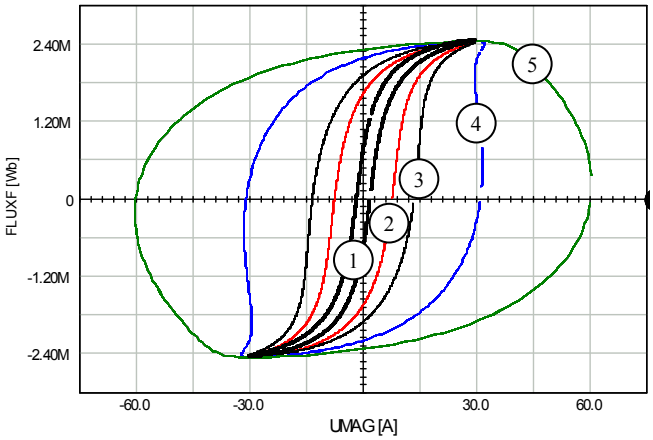

Fig. 11. Magnetization cycles at certain frequencies: 50Hz (1); 100Hz (2); 200Hz (3); 500Hz (4); 1kHz (5).

VI. Conclusion

The developed model considers nonlinear phenomena involved by the presence of the ferromagnetic core as main component of many electromagnetic devices, the study being focused on the nonlinear inductors. The model allows the time-domain simulation, so that any operation mode can be analyzed, including those that involve distorting operation modes, biases with DC or low-frequency premagnetization and minor magnetization loops. The model has been conceived in order to be implemented using powerful circuit simulators of SPICE family, capable to treat the whole circuit which includes one or more inductors. Our aim was mainly to overcome the well known difficulties related to the managing of the ferromagnetic hysteresis and the eddy-current effect, for design optimization purposes. The assessment of iron losses was carefully managed.

The given example certifies the capabilities of the developed model.

The obtained results can be extended for other engineering applications involving devices with ferromagnetic cores.

References

[1] M.C. Costa, S.I. Nabeta, J.R. Cardoso, *Modified Nodal Analysis Applied to Electric Circuits Coupled with FEM in the Simulation of a Universal Motor*, IEEE Transactions on Magnetics, vol. 36, no. 4, July 2000, pp. 1431-1434.

[2] R.Escarela-Perez, E. Melgoza, J.A.-Ramirez, *Systematic Coupling of Multiple Magnetic Field Systems and Circuits Using Finite Element*

ISBN: 978-988-19251-4-5
ISSN: 2078-0958 (Print); ISSN: 2078-0966 (Online)

and Modified Nodal Analyses, IEEE Transactions on Magnetics, vol. 47, no. 1, January 2011, pp. 207-213.

[3] L.O. Chua, K.. Stromsmoe, Lumped-Circuit *Models for Nonlinear Inductors Exhibiting Hysteresis Loops*, IEEE Transactions on Circuit Theory, vol. CT-17, no. 4, November 1970, pp. 564-574.

[4] J.H. Chan, A. Vladimirescu, X.C. Gao, P. Liebmann, J. Valainis, *Nonlinear Transformer Model for Circuit Simulation*, IEEE Transactions on Computer-Aided Design, vol. 10, no. 4, April 1991, pp. 476-482.

[5] J.T. Hsu, K.D.T. Ngo, *Subcircuit Modeling of Magnetic Cores with Hysteresis in PSpice*, IEEE Transactions on Aerospace and Electronic Systems, vol. 38, no. 4 October 2002, pp. 1425-1434.

[6] P.R. Wilson, J.N. Ross, A.D. Brown, *Simulation of Magnetic Component Models in Electric Circuits Including Dynamic Thermal Effects*, IEEE Transactions on Power Electronics, vol. 17, no. 1, January 2002, pp. 55-65.

[7] D.W.P. Thomas, J. Paul, O. Ozgonenel, C. Christopoulos, *Time-Domain Simulation of Nonlinear Transformers Displaying Hysteresis*, IEEE Transactions on Magnetics, vol. 42, no. 7, July 2006, pp. 1820-1827.

[8] L. Mandache, D. Topan, *Modeling and Time-Domain Simulation of Wired Ferromagnetic Cores for Distorted Regimes*, Buletinul Institutului Politehnic din Iaşi, Univ. Tehnică “Gh. Asachi”; Tomul LIV (LVIII), fasc. 3, 2008, Electrotehnică, energetică, electronică, pag. 303-310; ISSN 1223-8139.

[9] L. Mandache, D. Topan, K. Al-Haddad, *Modeling of Nonlinear Ferromagnetic Cores*, Revue Roumaine des Sciences Techniques, série Électrotechnique et Énergétique, Tome 53, No. 4, Bucarest, 2008, Ed. de l'Académie Roumaine, pp. 403-412.

[10] D.C. Jiles, J.B. Thoelke, M.K.Devine, *Numerical Determination of Hysteresis Parameters the Modeling of Magnetic Properties Using the Theory of Ferromagnetic Hysteresis*, IEEE Transactions on Magnetics, vol. 28, no. 1, January 1992, pp. 27-35.

[11] D.C. Jiles, D.L. Atherton, *Ferromagnetic Hysteresis*, IEEE Transactions on Magnetics, vol. MAG-19, No. 5, September 1983, pp. 2183-2185.

[12] D. Topan, L. Mandache, R. Süsse, Advanced Analysis of Electric Circuits, Wissenschaftsverlag Thüringen, Langenwiesen, 2011.

[13] ***, IsSpice4 User’s Guide, Intusoft co., San Pedro, Ca., 1995.

[14] M. Iordache, L. Mandache, M. Perpelea, *Analyse numérique des circuits analogiques non linéaires*, Ed. Groupe Horizon, Marseille, 2006.

ISBN: 978-988-19251-4-5
ISSN: 2078-0958 (Print); ISSN: 2078-0966 (Online)